arXiv:1109.3612v2 [cond-mat.mes-hall] 23 Sep 2011

Exciton-phonon coupling efficiency in CdSe quantum dots embedded in ZnSe nanowires

S. Bounouar[1,2], C. Morchutt[2], M. Elouneg-Jamroz[1,2], L. Besombes[1], R. André[1], E. Bellet-Amalric[2], C. Bougerol[1], M. Den Hertog[3], K. Kheng[2], S. Tatarenko[1], and J. Ph. Poizat[1]
[1] *CEA-CNRS-UJF group 'Nanophysique et Semiconducteurs', Institut Néel, CNRS - Université Joseph Fourier, 38042 Grenoble, France,*
[2] *CEA-CNRS-UJF group 'Nanophysique et Semiconducteurs', CEA/INAC/SP2M, 38054 Grenoble, France,*
[3] *Institut Néel, CNRS - Université Joseph Fourier, 38042 Grenoble, France,*

Exciton luminescence of a CdSe quantum dot (QD) inserted in a ZnSe nanowire is strongly influenced by the dark exciton states. Because of the small size of these QDs (2-5nm), exchange interaction between hole and electron is highly enhanced and we measured large energy splitting between bright and dark exciton states ($\Delta E \in [4, 9.2]$ meV) and large spin flip rates between these states. Statistics on many QDs showed that this splitting depends on the QD size. Moreover, we measured an increase of the spin flip rate to the dark states with increasing energy splitting. We explain this observation with a model taking into account the fact that the exciton-phonon interaction depends on the bright to dark exciton energy splitting as well as on the size and shape of the exciton wave function. It also has consequences on the exciton line intensity at high temperature.

PACS numbers: 78.67.Lt, 78.55.Et

I. INTRODUCTION

Semiconductor nanowires (NWs) have attracted great attention in the last few years since they hold great promise to become building blocks in tomorrow's nanoscale devices and circuits with vast potential applications ranging from nanoelectronics [1–3], optoelectronics (light emitting diodes [4, 5], nanolasers [6]), thermoelectrical energy conversion [7], to biological or chemical sensors [8]. Most of the NW growth methods allow for the variation of the chemical composition [9, 10] or doping [11] along the longitudinal or radial directions. This enables the fabrication of semiconductor heterostructures, and more specifically of quantum dots (QDs).

Single QDs have turned out to be excellent candidates for stable and efficient single photon sources [12–16]. Within this category, QDs embedded in NWs have already demonstrated single photon emission [17], even at relatively high temperature ($T = 220$K) [18]. Quest for efficient and eventually room temperature QD single photon sources requires a good understanding of the excitonic dynamics in such systems.

In a QD, exciton states are split by the electron hole exchange interaction into higher energy bright exciton states (BS) and lower energy dark states (DS) [19] with respective angular momentum of $J_z = \pm 1$ and $J_z = \pm 2$. In the present system, the energy splitting is relatively large, and has already been measured around $\Delta E = 6$ meV [20]. As exchange interaction in semi-conductor materials is proportional to the spatial overlap between the electron and hole wave functions, it is strongly enhanced in low dimensional objects. Values of $\Delta E \in [2, 4] meV$ have been measured in quantum wells [21] and it has been demonstrated that they can be even higher in quantum wires [22]. Extremely large splitting were calculated and observed [23] in colloidal QDs ($\Delta E \in [2, 20]$ meV). This is the result of very good confinement of the carriers owing to the small size of the QDs. Effects of the dark states on the QD luminescence become noticeable when $\Delta E \gg k_B T$, with k_B the Boltzmann constant and T the temperature [20, 24, 25]. We show that under non resonant pumping, the BS excitonic population leaks towards the DS that recombines non-radiatively, leading to a reduced excitonic light emission compared to the biexcitonic one. Transitions between the BS and DS states are due to hole spin flips assisted by phonons [26]. The speed of this processes depends essentially on the efficiency of the hole interaction with the phonon reservoir experienced by the QD [27].

In this paper, we show that the QD size can highly influence the QD phonon spectral density and modify the spin flip rates between the bright and dark exciton states. It not only has consequences on the exciton intensity at $T = 4$K but also at high temperatures.

The paper is organized as follows. The sample preparation and the setup are presented in section II. In section III the BS to DS energy splitting ΔE of several QDs is extracted using temperature dependent lifetime measurements. In section IV we present the experimental dependence of the spin flip rate versus ΔE, and suggest an explanation based on a theoretical model. These results are then used in section V to discuss the exciton to biexciton line intensity ratio as a function of ΔE and of the temperature.

II. SAMPLE AND SETUP

The nanowires are grown by molecular beam epitaxy using the vapor-liquid-solid technique [28]. The substrate is GaAs 100 with a ZnSe buffer. After dewetting of a thin layer of gold at 500°C, the growth is performed at 410°C. The nanowires have a diameter of 10 nm and a

length of 400 nm. The wire diameter (around 10 nm) is of the order of the bulk exciton Bohr diameter in CdSe (11nm), which means that the carriers in the QD are in the strong confinement regime. In order to study single QD, the nanowires are broken and dispersed on a silicon substrate by direct contact. High resolution transmission electron microscope (TEM) images revealed very small QD sizes, from 2 to 5 nm in the nanowire direction [29]. Other TEM experiments coupled to spectroscopy on other samples showed that this growth technique often led to ZnSe encapsulated QDs. Photoluminescence on as-grown samples is centered around 2,35eV with a dispersion of $\pm 0.07eV$.

The experimental apparatus is a time resolved microphotoluminescence experiment setup. The excitation source is a frequency doubled picosecond Ti sapphire laser emitting at a wavelength of $\lambda = 950/2 = 475$ nm (ie 2.6 eV). Nanowires luminescence is detected through a $\delta\lambda = 0.04$ nm (ie $\delta E = 0.2$ meV) resolution spectrometer on a charged coupled device (CCD) camera for spectra or on a low jitter (40ps) avalanche photodiode (APD) for time resolved measurements (60 ps time resolution for the whole set-up).

III. QD SIZE EFFECT ON THE EXCHANGE INTERACTION

Figure 1(a) shows typical spectrum obtained on a single nanowire. The two transitions correspond to exciton and biexciton (respectively denoted X and XX) and were identified using cross-correlation techniques [20]. The biexciton binding energy is measured around 20 meV. The four relevant states of a neutral QD are represented on figure 1(c). The exciton is splitted in two states (noted DS and BS) linked by spin flip transition rates noted γ_{sp1} and γ_{sp2}. The quantities Γ_X and Γ_{XX} are the radiative recombination rates of the bright exciton and the biexciton, and Γ_{NR} is the non radiative decay rate of the dark exciton. These quantities have been measured at $T = 4$ K on nine QDs as $1/\Gamma_X = 0.50 \pm 0.05$ ns, $1/\Gamma_{XX} = 0.30 \pm 0.05$ ns, and $1/\Gamma_{nr} = 5.0 \pm 0.5$ ns, where the error is the dispersion amongst QDs. An example of power dependence under pulsed excitation is shown in figure 1(b) evidencing the linear and quadratic behavior of the X and XX line intensity respectively. In all the investigated QDs, saturating intensity of the exciton emission is smaller than the biexciton, which is a signature of the strong influence of the dark exciton [24]. When $\Delta E \gg k_B T$, dark excitons cannot transit back to the bright state as there are no phonons available for such a spin flip and dark excitons are stored until recombining non radiatively. As a result, the photoluminescence of the exciton is less intense than that of the biexciton at saturation. The biexciton luminescence is not affected by the presence of the DS, whereas the exciton BS has a large probability to decay to the DS and not produce any photon. As spin flip rates are here of same order of magnitude or larger than the BS radiative decay, exciton intensity is generally small compared to the biexciton.

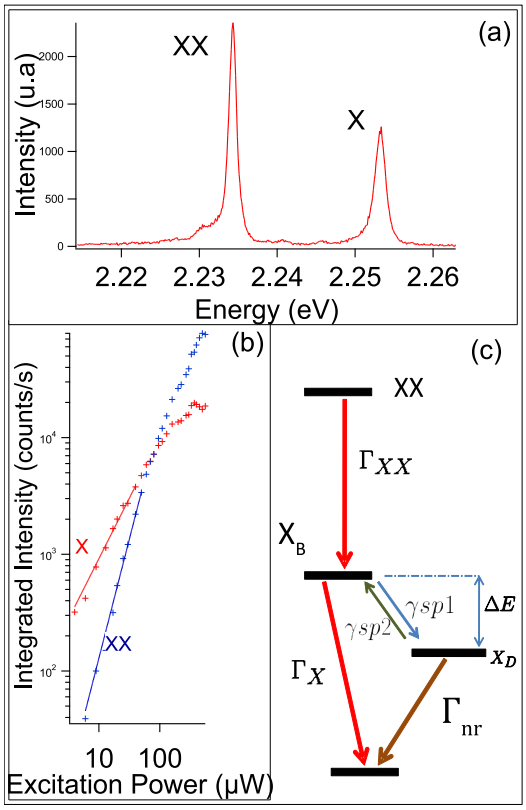


Figure 1: (Color online) (a) Spectrum of a neutral QD at $T = 4$ K. (b) Power dependence of the X and XX lines under pulsed excitation at $T = 4$ K. (c) Level scheme and transition rates of a neutral QD.

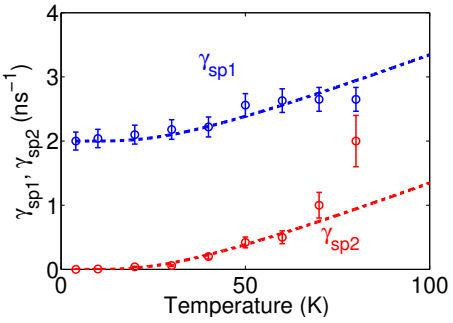


Figure 2: (Color online) Transition rates γ_{sp1} and γ_{sp2} versus temperature. The dashed lines are the plot from the theoretical model following phonon population evolution with temperature.

Temperature dependence of exciton decay time give access to the energy splitting ΔE between DS and BS [20, 25]. Spin flip transition rates depend on the spectral density of the acoustic phonons at the energy of the transition ΔE and on the phonon population that fol-

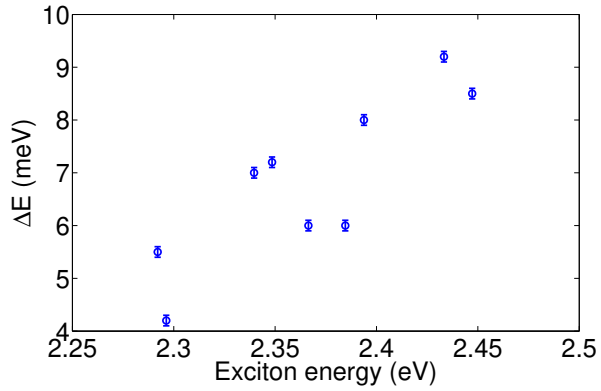


Figure 3: (Color online) Increase of splitting energies ΔE between DS and BS measured on nine QDs as a function of their excitonic emission energy.

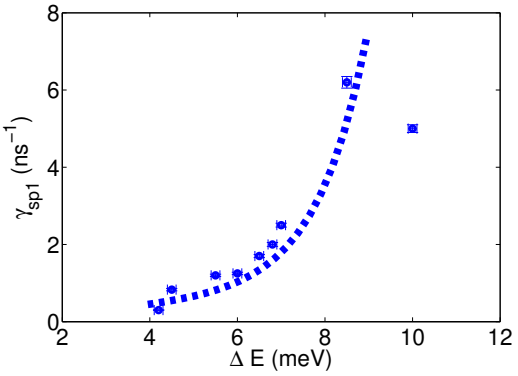


Figure 4: (Color online) Transition rate from BS to DS γ_{sp1} at 4K plotted as a function of splitting energy ΔE between DS and BS for nine differents QDs. The dotted line is a guide for the eyes.

lows a Bose-Einstein distribution $N_B(\Delta E, T) = 1/(1 - \exp(\Delta E/k_B T))$. The spin flip rates γ_{sp1} (bright to dark) and γ_{sp2} (dark to bright) can be written as:

$$\gamma_{sp1} \propto (N_B(\Delta E, T) + 1) R(\Delta E), \quad (1)$$
$$\gamma_{sp2} \propto N_B(\Delta E, T) R(\Delta E). \quad (2)$$

The quantity $R(\Delta E)$ depends on the BS-DS energy splitting ΔE but also on the spatial extension and shape of the wave function of the exciton[30, 31].

At $T = 0$K, $N_B = 0$, so that the spectral density $R(\Delta E) \propto \gamma_{sp1}(0K)$ represents the bright to dark state transition rate and $\gamma_{sp2} = 0$. When the temperature is increased so that $k_B T \sim \Delta E$, the bright exciton state is repopulated. For each temperature the transition rates γ_{sp1} and γ_{sp2} are extracted from the time resolved luminescence and their evolution is fitted using the model based on the level scheme of figure 1 (c)) with ΔE as the fitting parameter.

This process is repeated on nine QDs. As shown on figure 3, measured splittings range from 4.2 meV to 9.2 meV. A clear trend is appearing: splittings measured for low energy emission QDs are generally smaller compared to splittings measured for high energy emission QDs. The latters correspond to small size QDs, where electron and hole wave functions overlap very well, so that their exchange energy is large, leading to large ΔE. Such relationships between QD sizes and energy splittings have been calculated for colloidal QDs [32]. Change in composition of the $Cd_xZn_{1-x}Se$ QD can also affect the emission energy and the value of ΔE. Our measurements do not follow exactly a smooth law. The shape of the confinement has also a strong influence on the wave function forms, and consequently on their correlation function. For example the prolate or oblate nature of the QD geometry appears to have an important effect. This explains why we obtained a cloud of experimental points following a general trend instead of a strict dependence.

IV. EFFICIENCY OF THE EXCITON-PHONON COUPLING

In figure 4, we have plotted the transition rates from BS to DS measured at 4K, $\gamma_{sp1}(4K)$, versus energy splittings ΔE for nine different QDs. A clear enhancement of the transition rate for large ΔE can be observed. It can be also noted that the measured rates are comparable and even large than the excitonic radiative rate [24]. This is why the bright exciton is so depopulated compared to the biexciton in all the QDs investigated.

The results displayed in figure 4 indicate that large ΔE splittings lead to extremely fast depopulation of the bright state suggesting that exciton-phonon interaction becomes more efficient with large ΔE. As explained, larger splittings correspond to small QDs. Exciton coupling to phonons not only depends on the energy needed for the spin flip but also on the QD size. But size and ΔE are not independent parameters and induce opposite effects on the transition rates. In order to explain this non-trivial behavior, it is necessary to calculate the phonon spectral density as a function of QD size and energy splitting ΔE for each particular QD to obtain a general trend.

We shall only consider longitudinal acoustical (LA) compression modes since longitudinal optical (LO) phonons have energies of about 30 meV far above the dark - bright exciton splitting ΔE. In the following we will perform this calculation both in the 3D and in the 1D case for the available phonon modes. The NW geometry is obviously somewhere in-between these two extreme cases that will only give us a qualitative behavior.

We first consider the 3D situation. The phonons dispersion is bulk-like, approximated by the Debye law $w(k) = c_l k$, with c_l the sound speed for LA phonons in the semiconductor material. Piezoelectric interactions and Fröhlich longitudinal optical (LO) phonon couplings

are neglected. The exciton-phonon interaction is dominated by the hole-phonon interaction [26]. We therefore consider only the latter, whose Hamiltonian can be written, in the second quantization representation with respect to the carrier states, as:

$$H_h = \frac{1}{\sqrt{N}} \sum_{knn'} a_n^\dagger a'_n f_{h,nn'}(k)(b_k + b_{-k}), \tag{3}$$

where $a_n^\dagger$ and a_n are the hole creation and annihilation operators, $b_k^\dagger$ and b_k are LA phonon creation and annihilation operators. The index n represents the excitation level of the hole, and k the phonon mode. The coupling constant is defined as

$$f_{h,nn'}(k) = \sigma_h \sqrt{\frac{\hbar k}{2\rho V c_l}} F_{nn'}(k), \tag{4}$$

where σ_h is the deformation potential for holes, V is the unit cell volume, ρ is the CdSe volumic mass. The quantity $F_{nn'}(k)$ is a purely geometrical form factor given by [27] :

$$F_{nn'}(k) = \int_{-\infty}^{\infty} d^3 r \psi_n^*(r) e^{ikr} \psi_{n'}(r). \tag{5}$$

In order to evaluate the coupling constant for the lowest hole state $f_{11}(E)$ we consider the harmonic oscillator potential ground state as the wave function of the hole:

$$\psi(r) = \frac{1}{\pi^{3/4} l_\perp \sqrt{l_z}} \exp\left[-\frac{1}{2}\left(\frac{r_\perp}{l_\perp}\right)^2 - \frac{1}{2}\left(\frac{z}{l_z}\right)^2 \right], \tag{6}$$

where $r_\perp$ is the position component in the xy plane and $l_\perp, l_z$ are respectively the in plane, and out of plane (z direction) localization widths. For this wave function the form factor is easily found as

$$F_{11}(k) = \exp\left[-\left(\frac{k_\perp l_\perp}{2}\right)^2 - \left(\frac{k_z l_z}{2}\right)^2 \right]. \tag{7}$$

For the lowest hole state, the phonon spectral density in the QD is:

$$\begin{aligned} R(E) =& \frac{1}{\hbar^2}(N_B(E)+1) \\ & \times \frac{1}{N} \sum_k F_{11}(k) F_{11}^*(k) [\delta(E - E(k)) + \delta(E + E(k))]. \end{aligned} \tag{8}$$

After performing the summation over k in the continuum limit, introducing the quadratic density of state of the phonons corresponding to the 3D case, the phonon spectral density is :

$$R(E) = R_o E^3 g(E), \tag{9}$$

with

$$R_o = \frac{(\sigma_h)^2}{8\pi^2 \hbar \rho c_l^5}. \tag{10}$$

The quantity R_o contains all material parameters. The cubic dependence is due to the quadratic phonon density of state, and the function g(E) is a function of the energy and of the geometrical parameters of the QD [33]:

$$\begin{aligned} g(E) = \int_{-\frac{\pi}{2}}^{\frac{\pi}{2}} \zeta \cos\zeta \exp\left[-\frac{(l_\perp)^2 E^2}{2\hbar^2 c_l^2} \right. \\ \left. \times \left(cos^2\zeta + \frac{l_z^2}{(l_\perp)^2} sin^2\zeta \right) \right] d\zeta, \end{aligned} \tag{11}$$

where ζ is the angle of the wave vector k with respect to the normal to the z direction.

Describing coupling of the hole to phonons confined in a nanowire the same way as in a 3D semi conductor bulk matrix seems a rough approximation. So we also considered the 1D case in which the nanowire is taken as an infinitely thin monomode wave guide. The phonon density of state is constant and we consider that only the phonons propagating along the nanowire (z direction) can couple to the hole whose wavefunction is taken as $\psi_h(r) \propto \exp[-(1/2)(z/l_z)^2]$. The spectral density becomes:

$$R_{1D}(E) \propto E g_{1D}(E), \tag{12}$$

with

$$g_{1D}(E) = \exp\left[-\frac{l_z^2 E^2}{2\hbar^2 c_l^2} \right]. \tag{13}$$

The phonon spectral density is linear with energy but the geometrical factor $g_{1D}(E)$ has the same gaussian energy dependence as g(E).

Since at T = 4K, $\gamma_{sp1}(4K) \propto R(\Delta E)$, the BS to DS spin flip rate evolution from dot to dot can be described by calculating the phonon spectral density for each QD. Three calculated 3D phonon spectral densities corresponding to three different l_z values ($l_z = 2, 4, 6$ nm) are plotted in figure 5(a). Because of its increase with energy (linear for 1D, cubic for 3D), $R(\Delta E)$ corresponding to QDs with smaller l_z have their maximum enhanced and shifted toward the higher energies. As a consequence, in small QDs, high energy phonons couple more efficiently with the hole. We propose to explain qualitatively the increase of the transition rate observed in figure 4 by this size effect.

The hole-phonon coupling efficiency, $R_{l_z}(\Delta E)$ depends on the QD size l_z and on the energy splitting ΔE. We determine the relation between l_z and ΔE by evaluating the short range hole-electron exchange energy in the QD:

$$\Delta E = \Delta E^{3d} \frac{1}{|\varphi^{3d}(0)|^2} \int |\psi_e(r)|^2 |\psi_h(r)|^2 d^3 r, \tag{14}$$

where $\psi_{e/h}(r)$ are the electron/hole wave functions, ΔE^{3d} is the exchange energy in the bulk material ZnCdSe [34] ($\Delta E^{3d} = 0.19$ meV, for a $Cd_{0.5}Zn_{0.5}Se$ composition of the QD as measured in high resolution TEM experiments [29]), and $|\varphi^{3d}(0)|^2 = 1/\pi a_B^{*3}$ with a_B^* the Bohr radius of the free exciton. To match the measured values of ΔE (from 4 meV to 9 meV), we set the lateral

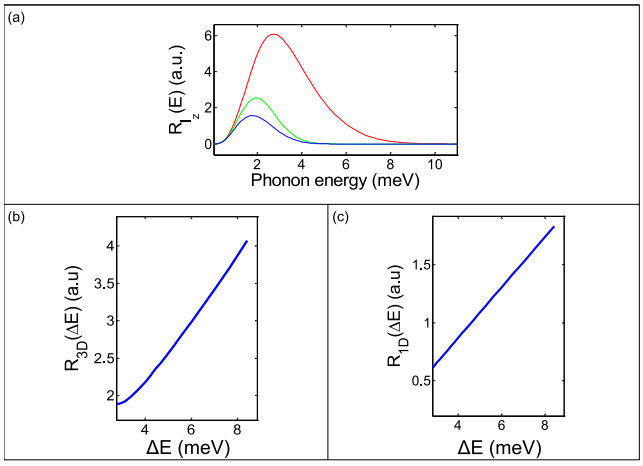


Figure 5: (Color online) (a) 3D Phonon spectral density for 3 different QD sizes along the z direction (red curve: l_z =2 nm, green curve: l_z=4 nm, blue curve: l_z=6 nm). Smaller QD z dimension shifts the maximum of the coupling constant toward the higher energies, and enhances its relative value. (b) Calculated 3D hole-phonon coupling efficiency vs transition energy ΔE. (c) Calculated 1D hole-phonon coupling efficiency vs transition energy ΔE.

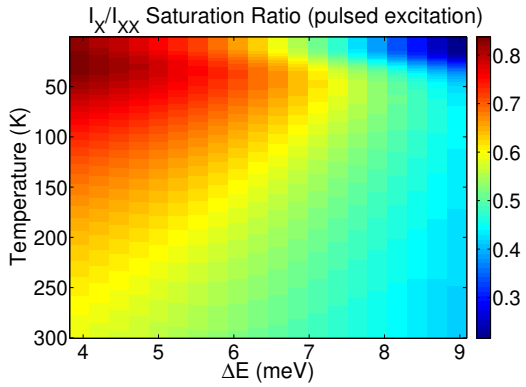


Figure 6: (Color online) Calculated saturation ratio Ix/Ixx under pulsed excitation as a function of ΔE and temperature. The color legend represents Ix/Ixx saturation ratio. The cold colors show low exciton intensity and the hot color high intensity.

confinement parameter $l_\perp$ at 4nm. With l_z linked to a corresponding ΔE we make l_z vary from 2 nm to 6 nm and we calculate $R_{l_z}(\Delta E)$.

The results, for the 3D and 1D cases described above, are plotted in figure 5 (b) and (c). Because of the simplicity of the considered exciton wave function, the aim of the calculation is neither to fit the experimental data nor to obtain a quantitative estimation of the transition rates. However, we can show that the hole-phonon coupling efficiency is increasing with ΔE in both cases, which is not

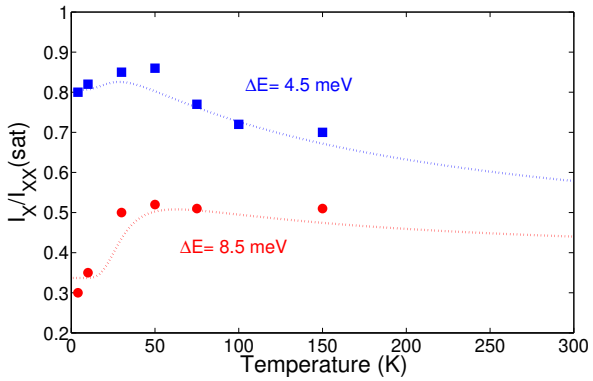


Figure 7: (Color online) Experimental exciton-biexciton saturation ratio under pulsed excitation versus temperature for two QDs with respectively $\Delta E = 4.5$ meV (blue squares) and $\Delta E = 8.5$ meV (red circles). Dashed lines are vertical cut (fixed ΔE) from the model used in figure 6.

a trivial result as the cut-off imposed by the dimensions of the QD makes this efficiency vanish for higher energy phonons. The effect of the confinement dimensions on the phonon spectral density can be a good explanation for the trend measured by the experiment in figure 4. The two situations considered here are extreme cases and we can expect a real nanowire geometry to impose an intermediate behavior for the hole phonon coupling.

V. EXCITON LUMINESCENCE INTENSITY

This increase of the exciton-phonon coupling efficiency with energy splitting has some consequences on the temperature dependent exciton-biexciton saturation ratio under pulsed excitation. This calculated ratio is represented in figure 6 as a function of temperature and energy splitting ΔE. We used the level scheme presented in figure 1 and the values of the transition rates given in section III. The relation between $\gamma_{sp1}(4K)$ and ΔE is taken from the function used as a guide for the eyes in figure 4. We also considered the increase of the dark exciton non radiative recombination $\Gamma_{nr}(T)$ with temperature following an Arrhenius law $\Gamma_{nr}(T) \sim exp(-E_a/k_BT)$, with an activation energy E_a. For the two QDs studied in fig. 7 we have measured $E_a = 30 \pm 5$ meV and we have taken $E_a = 30$ meV in the model used in figures 6 and 7. The particularity here is that the DS lifetime at $T = 4$ K ($1/\Gamma_{nr} = 5$ ns) is very short compared to values reported in other systems (up to $1\mu s$ [25]) and is of the same order of magnitude as the exciton radiative lifetime when temperature is raised up to only several tens of K. A characteristic temperature behavior is shown in figure 6. The exciton intensity is very small at low temperature (particularly in the high splitting region), increases as temperature is increased up to $T = 50$ K, and finally decreases with higher temperatures. The effect of repop-

ulation of the bright exciton due to the DS to BS spin flip is compensated and overwhelmed by the exciton population loss caused by the faster dark exciton non radiative recombination. As shown in figure 7, representing the exciton-biexciton ratio versus temperature for 2 different QDs with different measured ΔE (4.5 meV and 8.5 meV), this exciton line intensity decrease is more sensitive for large ΔE. However, at 300K, the bright exciton is still less luminescent for large splittings. It can be noted that the model fits rather well the experimental data.

VI. CONCLUSION

In summary, the exciton-phonon coupling efficiency is highly influenced by the QD size. This can explain the observed enhancement of the bright to dark spin flip rate with increasing splitting energy. As a result, the saturation intensity of exciton transition is a lot weaker than the biexciton one. This effect is all the more important as the QD exchange splitting ΔE is larger. The domination of the biexcitonic line over the excitonic line is preserved at high temperature despite the bright state repopulation owing to the temperature induced loss of excitonic population through the non radiative dark exciton recombination. This exciton weakness could suggest to use the biexciton line for high temperature single photon sources. In that case, the contamination by the exciton line could be reduced when the lines are broadened at high temperature.

VII. ACKNOWLEDGEMENTS

We acknowledge support from the French National Research Agency (ANR) through the Nanoscience and Nanotechnology Program (Project BONAFO ANR-08-NANO-031-01) that provided a research fellowship for MdH. MEJ acknowledges financial support from the Nanosciences Foundation "Nanosciences, aux limites de la nanoélectronique" (RTRA).

[1] X. Duan, Y. Huang, Y. Cui, J. Wang, and C. M. Lieber, Nature **409**, 66 (2001)
[2] W. Lu and C. M. Lieber, Nature Materials **6**, 841 (2007)
[3] C. Thelander, T. Martensson, M. T. Björk, B. J. Ohlsson, M. W. Larsson, L. R. Wallenberg, and L. Samuelson, Appl. Phys. Lett. **83**, 2052, (2003).
[4] R. Könenkamp, R.C. Word, and C. Schlegel Appl. Phys. Lett. **85**, 6004 (2004)
[5] H. M. Kim, Y. H. Cho, H. Lee, S. I. Kim, S. R. Ryu, D. Y. Kim, T. W. Kang, and K. S. Chung, Nano Lett. **4**, 1059 (2004)
[6] X. Duan, Y. Huang, R. Agarwal, and C. M. Lieber, Nature **421**, 241 (2003)
[7] A. I. Hochbaum, R.Chen, R. D. Delgado, W. Liang, E. C. Garnett, M. Najarian, A. Majumdar, and P. Yang, Nature **451**, 163 (2008)
[8] Y. Cui, Q. Wei, H. Park, and C. M. Lieber, Science **293**, 1289 (2001)
[9] M. S. Gudiksen, L. Lauhon, J. Wang, D. C. Smith, and C. M. Lieber, Nature **415**, 617 (2002)
[10] M. T. Björk, B. J. Ohlsson, T. Sass, A. I. Persson, C. Thelander, M. H. Magnusson, K. Deppert, L. R. Wallenberg, and L. Samuelson, Nanoletters **2**, 87 (2002); Appl. Phys. Lett. **80**, 1058 (2002)
[11] C. Yang, Z. Zhong, and C. M. Lieber, Science **310**, 1304 (2005)
[12] P. Michler, A. Kiraz, C. Becher, W. V. Schoenfeld, P. M. Petroff, L. Zang, E. Hu, and A. Imamoglu, Science **290**, 2282 (2000).
[13] E. Moreau, I. Robert, J.-M. Gérard, I. Abram, L. Manin, and V. Thierry-Mieg, Appl. Phys. Lett. **79**, 2865 (2001).
[14] C. Santori, D. Fattal, J. Vučković, G. S. Solomon, and Y. Yamamoto, Nature **419**, 594 (2002).
[15] W. H. Chang, W. Y. Chen, H. S. Chang, T. P. Hsieh, J. I. Chyi, and T. M. Hsu, Phys. Rev. Lett. **96**, 117401 (2006).
[16] J. Claudon, J. Bleuse, N. S. Malik, M. Bazin, P. Jaffrennou, N. Gregersen, C. Sauvan, P. Lalanne, and J.-M. Gérard, Nature Photonics **4**, 174 (2010)
[17] M. T. Borgström, V. Zwiller, E. Müller, and A. Imamoglu, Nano Lett. **5**, 1439 (2005)
[18] A. Tribu, G. Sallen, T. Aichele, R. André, C. Bougerol, S. Tatarenko, J.-Ph. Poizat, and K. Kheng, Nanoletters **349**, 225 (1991).
[19] V. D. Kulakovskii, G. Bacher, R. Weigand, T. Kümmell, A. Forchel, E. Borovitskaya, K. Leonardi and D. Hommel, Phys. Rev. Lett. **82**, 1780 (1999); L. Besombes, K. Kheng, and D. Martrou, Phys. Rev. Lett. **85**, 425 (2000).
[20] G. Sallen, A. Tribu, T. Aichele, R. André, L. Besombes, C. Bougerol, S. Tatarenko, K. Kheng, and J.-Ph. Poizat, Phys. Rev. B **80**, 085310 (2009).
[21] Y. Chen, B. Gil, P. Lefebvre, and H. Mathieu, Phys. Rev. B **37**, 6429 (1988).
[22] Y. Chen, Phys. Rev. B **41**, 10604 (1990).
[23] M. Nirmal, D. J. Norris, M. Kuno, M. G. Bawendi, Al. L. Efros, and M. Rosen, Phys. Rev. Lett. **75**, 3728 (1995).
[24] M. Reischle, G. J. Beirne, R. Rossbach, M. Jetter, and P. Michler, Phys. Rev. Lett. **101**, 146402 (2008).
[25] O. Labeau, P. Tamarat, and B. Lounis, Phys. Rev. Lett. **90**, 257404 (2003).
[26] L. M. Woods, T. L. Reinecke, and R. Kotlyar, Phys. Rev. B **69**, 125330 (2004)
[27] A. Grodecka, L. Jacak, P. Machnikowski, and K. Roszak, arXiv:cond-mat/0404364 (2004).
[28] M. Den Hertog, M. Elouneg-Jamroz, E. Bellet-Amalric, S. Bounouar, C. Bougerol, R. André, Y. Genuist, J.-Ph. Poizat, K. Kheng and S. Tatarenko, J. Crystal Growth **323**, 330 (2011)
[29] M. Den Hertog, M. Elouneg-Jamroz, E. Bellet-Amalric, S. Bounouar, C. Bougerol, R. André, Y. Genuist, J.-Ph. Poizat, K. Kheng and S. Tatarenko, J. Appl. Phys. **110**, 034318 (2011).

[30] L. Besombes, K. Kheng, L. Marsal, and H. Mariette, Phys. Rev. B **63**, 155307 (2001).
[31] T. Takagahara, Phys. Rev. B **60**, 2638 (1999)
[32] Al. L. Efros, and M. Rosen, M. Kuno, M. Nirmal, D. J. Norris, and M. Bawendi, Phys. Rev. B **54**, 4843 (1996).
[33] A. Grodecka, C. Weber, P. Machnikowski, and A. Knorr, Phys. Rev. B **76**, 205305 (2007)
[34] J. Puls, F. Henneberger, M. Rabe, and A. Siarkos, Journal of Crystal Growth **184/185**, 787 (1998)